THE JOURNAL OF PHYSICAL CHEMISTRY C

ARTICLE

pubs.acs.org/JPCC

External Electric Field Manipulations on Structural Phase Transition of Vanadium Dioxide Nanoparticles and Its Application in Field Effect Transistor

W. W. Li,[†] J. J. Zhu,[†] J. R. Liang,[‡,∥] Z. G. Hu,[*,†] J. Liu,[†,§] H. D. Chen,[‡] and J. H. Chu[†]

[†]Key Laboratory of Polar Materials and Devices, Ministry of Education, Department of Electronic Engineering, East China Normal University, Shanghai 200241, China

[‡]State Key Laboratory on Integrated Optoelectronics, Institute of Semiconductors, Chinese Academy of Sciences, Beijing 100083, China

[§]State Key Laboratory for Superlattices and Microstructures, Institute of Semiconductors, Chinese Academy of Sciences, Beijing 100083, China

[∥]School of Electronic and Information Engineering, Tianjin University, Tianjin 300072, China

ABSTRACT: Despite the intensive study on the famous metal−insulator transition, many questions regarding the evolution of the structural phase transition (SPT) in vanadium dioxide (VO_2) remain unresolved. Here, the lattice vibrations and SPT of VO_2 nanoparticles on a SiO_2/Si(100) substrate with different applied voltage from 0 to 8 V have been investigated by Raman scattering spectra. It can be found that both the intensities of the A_g and B_g phonon modes decrease with increasing temperature. Moreover, the vibration modes disappear when heating up to the temperature of SPT (T_{SPT}). With the voltage increasing from 0 to 8 V, the T_{SPT} decreases from 68.3 to 64.3 °C for the heating process and from 66.3 to 58.8 °C for the cooling process, respectively. The fitting results reveal that the T_{SPT} was decreased by −0.48 and −0.87 °C/V in the heating and cooling processes, respectively. This is because the larger electric field could assist the shortening of the V−V distance and the change of carriers between electrons and the mixing of electrons and holes. Moreover, the T_{SPT} delay was increased by 0.4 °C/V with increasing the positive voltage because the electric field can pull the electrons and push the holes. The present results of the VO_2 three-terminal device show a potential realization of the VO_2-based field effect transistor.

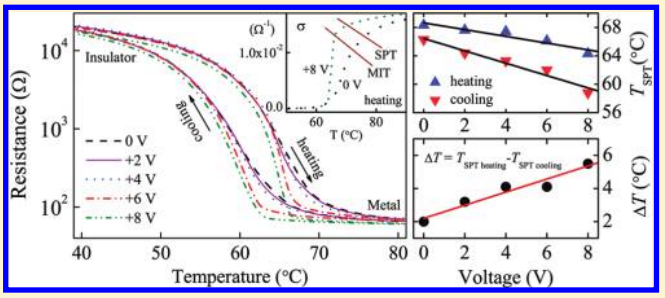

INTRODUCTION

Complex transition metal oxides that are able to switch intrinsic electronic and magnetic properties in response to an extrinsic stimulus are of significant interest to condensed matter physics.[1,2] The atomic and/or electronic reconstruction at grain boundaries or doping centers in these oxides enriches the electronic phases.[3] In particular, vanadium dioxide (VO_2) undergoes a metal−insulator transition (MIT) at about 68 °C accompanied by a structural phase transition (SPT) from high-temperature tetragonal rutile (R) phase to low-temperature monoclinic (M) phase, where pairing and tilting of V^{4+} cations result in chains with alternating long and short V−V distance along the *c* axis. At the MIT temperature, the opening of a band gap in the mid-infrared optical conductance and a jump of several orders of magnitude in the resistivity are observed.[4−6] These features make VO_2 a promising material for applications in high-gain switching, thermal relay device, and optical storage elements. Involving various electronic degrees of freedom (charge, orbital, and spin) and their coupling to the lattice degrees of freedom (phonons),[7] the MIT of VO_2 has been shown to be affected by doping,[8] stress,[9,10] and electric field.[11,12] Among them, the external electric field is expected to be an acceptable and advanced method because of its evident advantages such as low cost, simplicity, and precise control. Using the phase transition-induced resistance change and/or nonlinear current−voltage characteristics, electric field triggering MIT in VO_2 is promising for potential applications as ultrafast switches, Mott field effect transistor, and two-terminal memristive devices.[13,14] Furthermore, it can provide a critical carrier density and lead to the phase transition. Therefore, it is of fundamental scientific interest to investigate the physical properties behind the electrically induced phase transition.

A recent report reveals that the MIT with a change in on-site Coulomb interaction could occur without the accompanying SPT and an intermediate phase between the MIT and SPT was observed.[15,16] It first undergoes a large resistance change (regarded as the MIT) near critical temperature (T_{MIT}) and then a SPT between the M and R structure, which indicates that the T_{MIT} is lower than the temperature of SPT (T_{SPT}). Many research works have been focused on the physical mechanisms of MIT and the modifications of T_{MIT} by adding an external

Received: July 28, 2011
Revised: September 26, 2011
Published: October 24, 2011

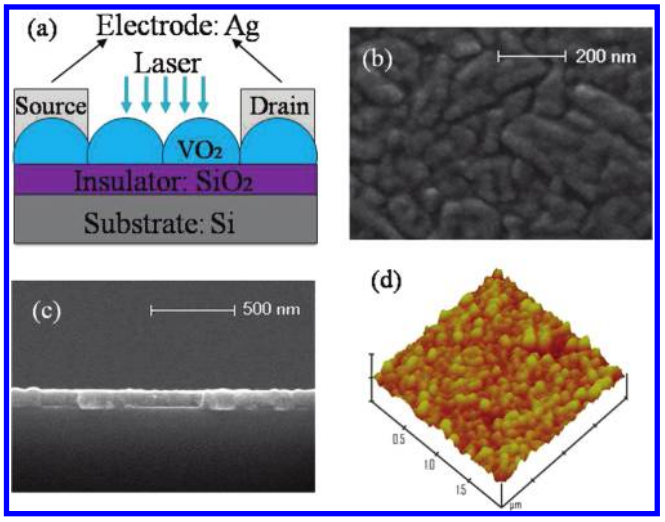

Figure 1. (a) Schematic representation of the device (or transistor) to probe the structural phase transition. Surface (b) and cross-sectional (c) SEM images of the VO_2 nanoparticles. (d) AFM three-dimensional image. The scale height is 50 nm and the measured area is $2 \times 2\ \mu m^2$.

electric field at the fixed temperature. For example, voltage-triggered MIT has been observed at room temperature (RT) with the threshold voltage of 2.1 V for VO_2 films.[13] In the heating process, the T_{MIT} discerned from the current−temperature curves of VO_2 films strongly depends on the external electric field.[17] However, there are some limited data on the SPT of VO_2 especially exploring electric field effects. Considering the hysteresis effects of conductance in VO_2, the T_{SPT} under an electric field should be remarkably discrepant with heating and cooling across the SPT.

The Mott phase transition of VO_2 materials is related to grains and grain boundaries. Nanoscale samples have the smaller characteristic domain size. In particular, the nanoscale VO_2 materials in a single crystal contain an extremely low level of defects and impurities for heterogeneous nucleations and can remain single-domain across the phase transition.[18,19] So the intrinsic property of individual phases can be obtained. In addition, the size at such length scales could have significantly altered the electronic and structural components of the transition due to modification of the surface energies.[20] Low-dimensional VO_2 nanostructures not only provide a new perspective to explore, understand, and ultimately engineer SPT for optoelectronic devices such as a field effect transistor but also improve the uniformity, reproducibility, and the controlling level of the SPT. It is desirable to carry out a delicate study on the relationship between the SPT and external electric field. Raman scattering has been known to be an excellent nondestructive tool to study the physical transition, chemical composition, and lattice dynamics of various nanomaterials.[21,22]

In this article, VO_2 nanoparticles were fabricated by direct-current magnetron sputtering on a SiO_2/Si substrate. The lattice vibrations and SPT of VO_2 nanoparticles have been investigated under different electric fields using Raman spectra. Temperature and electric field dependences of the resistance have been simultaneously measured to confirm the spectroscopic results. The effects from the applied electric field on the T_{SPT} and the physical mechanism have been discussed in detail.

EXPERIMENTAL DETAILS

Fabrication of the VO_2 Nanoparticles. The SiO_2 film as a buffer layer were first prepared on the Si(100) substrate by plasma-assisted chemical vapor deposition. Then, the VO_2 nanoparticles were deposited using direct-current magnetron sputtering in an argon−oxygen atmosphere at RT on the SiO_2 film. Two vanadium metal disks with a high purity of 99.94% were placed face to face vertically as sputtered targets. The total gas pressure and sputtering power during the deposition was maintained at 6×10^{-2} Pa and 88 W, respectively. The target was presputtered for several minutes to clean their surfaces. Finally, the sample was annealed at 400 °C in nitrogen ambience by a thermal annealing process for 2 h. A more detailed growth process of the VO_2 nanoparticles can be seen elsewhere.[23,24]

Characterization of the VO_2 Nanoparticles. The surface morphology and cross-sectional microstructures of the VO_2 nanoparticles were characterized by atomic force microscopy (AFM) and scanning electron microscopy (SEM). A schematic representation of the three-terminal device (or transistor) is shown in Figure 1a. SiO_2 as the gate insulator was thermally treated and the SiO_2 insulator is strong with respect to a high field for electronic application. Silver (Ag) electrodes were prepared for Ohmic contact. The device was mounted into a Linkam THMSE 600 heating stage for variable temperature experiments from 10 to 100 °C. The temperature of the sample can be controlled within the accuracy of 0.1 °C, and the possible oxidation of the device during the heating and cooling process can be avoided under nitrogen atmosphere. A Keithley 2400 source meter was used to apply an external direct-current voltage to the VO_2 nanoparticles via Ag electrodes, and the resistance value can be recorded. The applied voltage was varied from 0 to 8 V with an interval of 2 V. Raman scattering experiments were carried out by a micro-Raman spectrometer (Jobin-Yvon Lab-RAM HR 800 UV) with a spectral resolution less than 1 cm^{-1}. A 488 nm Ar^+ laser beam with the power of 3 mW, which was used to minimize local heating of the sample, was incident on the VO_2 nanoparticles between the Ag electrodes, as plotted in Figure 1a.

RESULTS AND DISCUSSION

Surface Morphology and Cross-Section Characterization. The crystalline structure of the VO_2 sample has been analyzed by X-ray diffraction (XRD) previously.[24] There are the diffraction peaks (011), (211), and (220), and no impurity phases were observed, which indicates that the sample is of the monoclinic phase (not shown). The VO_2 nanoparticles were fabricated on a SiO_2/Si substrate using direct-current magnetron sputtering. The nanostructured VO_2 materials can strongly affect the optical and electrical properties of the transistor device. Figure 1b and d show the surface morphology of the VO_2 nanoparticles. The average grain size is estimated to about 100 nm. Owing to the diffusing effect, the distributions of the nanoparticles and their distances are not so uniform. To determine the detailed interfacial characteristics of the VO_2/SiO_2 layers, the cross-sectional SEM image was measured as shown in Figure 1c. The thicknesses of the SiO_2 and VO_2 layers are estimated to about 80 and 120 nm, respectively. The VO_2 nanoparticles are believed to gradually disperse after sputtering so the bottom side walls connect each other and can not be clearly identified.

Electric Properties with the External Voltage. The temperature dependence of the resistance at the voltage from 0 to 8 V

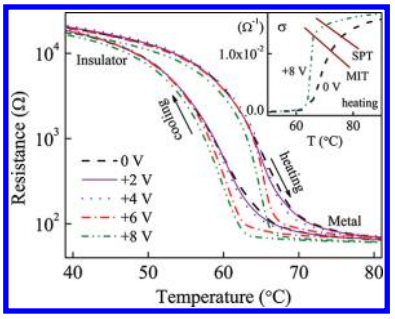

Figure 2. Temperature dependence of the resistance in the VO_2 nanoparticles at the electric voltage of 0, 2, 4, 6, and 8 V, respectively. Arrows on the curves denote the temperature sweep directions. The resistance is measured when the voltage is applied between two Ag electrodes straddling the VO_2 nanoparticles. The inset shows the electric conductance variations when heating across the MIT and SPT at the voltages of 0 and 8 V, respectively.

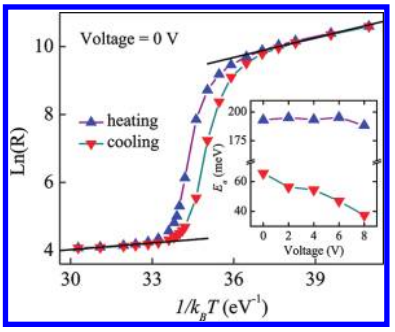

Figure 3. Plot of logarithmic resistance $\ln(R)$ vs $1/k_BT$ of the VO_2 nanoparticles at a voltage of 0 V. The inset shows the electric voltage dependence of the activation energy E_a at the high-temperature conducting states (red upside down triangle) and the low-temperature insulating states (blue triangle).

is displayed in Figure 2, and the 3 orders of magnitude change in the resistance can be observed. Moreover, the hysteresis loop of the resistance in VO_2 nanoparticles occur within a more narrow temperature window compared to that observed in films. The decrease in the resistance up to the transition temperature indicates an increase in the hole carriers, and two kinds of electron and hole carriers coexist near the transition temperature. In the high temperature metal regime, the free-carriers are electrons.[25] As the applied voltage increases from 0 to 4 V, the transition temperatures slightly shift toward lower temperature for both the heating and cooling processes. Then, the transition temperature remarkably decreases with further increasing of the voltage. This is because the external electric field and temperature can control the free-carrier densities. A low concentration of generated holes with the voltage drive the transition occurring.[17] It should be noted that the gating voltage actually sharpens the transition edge. At the structural transitions, the lattice shrinks along c_R and expands along a_R and b_R.[26] Hence, the increasing of applied electric voltage can accelerate the change of the lattice parameters, resulting in the sharp trends with the voltage in transition edge. As shown in the inset of Figure 2, the device first undergoes an abrupt conductance (σ) jump corresponding to the MIT. Further, the large drop region in the resistance compared with the insulating phase reveals a metallic-like behavior, corresponding to the intermediate phase. Finally, the electric conductivity gradually increases to the maximum, which can be assigned as the SPT. Therefore, the $\sigma-T$ curves can be divided into three regions: the insulating M phase, the intermediate phase, and the tetragonal R phase. Furthermore, both the T_{MIT} and T_{SPT} linearly decrease to different magnitudes with increasing electric voltage in the heating and cooling processes, thus widening the hysteresis of the transition.

There are many researches on discussing the origins of the insulator and intermediate phases. With increasing the temperature, the VO_2 nanobeams transform from the insulating monoclinic M_1 ($P2_1/c$) phase to a mixture of the Mott-insulating M_2 ($C2/m$) and metallic rutile phases.[27] However, Mun et al. determined that the low-temperature insulating state of VO_2 single crystals is the monoclinic M_2 structure. The intermediate phase is a mixture of the monoclinic M_2 and monoclinic M_1 structures, before the transition to the rutile state. The authors propose that the presence of internal strain in the VO_2 single crystals may contribute to the different transition process.[28] In addition, the observation that the MIT does not coincide with the SPT can be explained as the M_1 structure forming the M_2 structure, Therefore, the delocalized vanadium d-electrons of one sublattice are available to conduct, despite the lack of any apparent rutile structure. Obviously, the phase transition process explanation of the VO_2 materials, which is far away from satisfaction, depends on many factors, such as microstructure, crystalline orientation, stress/strain, and grain size, etc. In order to clarify the phenomena, it is necessary to further investigate the actual phase appearing in different VO_2 structures.

Electric Field Effects on the Activation Energy. The electric voltage dependence of the activation energy (E_a) can provide important information about the electronic band structure and free-carrier current. For insulators such as VO_2 at low temperature, E_a is the difference between the conduction band edge and the Fermi level, which is located in the middle of the gap.[29] Further, the activated behavior can reflect an energetic cost of carrier delocalization. The E_a value is estimated by the slope of a linear fitting of $\ln(R)$ over $(1/k_BT)$, as $\ln(R) = b + E_a/k_BT$, where R, T, k_B, and b is the resistance, temperature (in unit K), Boltzmann constant, and intercept, respectively. As an example, the logarithmic resistance $\ln(R)$ versus $1/k_BT$ at voltage of 0 V and the linear fitting are plotted in Figure 3. On the basis of the fitting results, the E_a values with the electric voltage are presented in the inset of Figure 3. It can be found that the E_a values (188−195 meV) at the low-temperature insulating state are remarkably larger than that (37−56 meV) at the high-temperature conducting state. This is because the high-temperature state is a mixture of metallic regions and some insulating phases due to the mixed valence states of the VO_2 nanoparticles. The values for both the high-temperature metallic state and the low-temperature insulating state are less than that found from VO_2 films (149 and 250 meV, respectively),[13,29] suggesting that nanoparticle formation could be helpful to activate the transition. Owing to the smaller characteristic domain size, the alternating SPT domain patterns spontaneously form along the nanoparticles axis, which can affect the changes in resistance with the temperature around the SPT. In addition, the fact that the imperfections such as oxygen vacancies and/or vanadium interstitials exist in the present nanoparticles could be another possible cause. Note that the E_a at both the insulating state and the metallic state decrease with increasing the voltage. It indicates that the transition can be easily activated under an external electric field, which could further affect the SPT of the VO_2

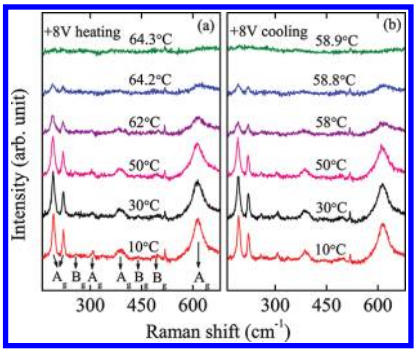

Figure 4. Raman spectra at different temperatures under an electric voltage of 8 V while (a) heating and (b) cooling across the structural phase transition.

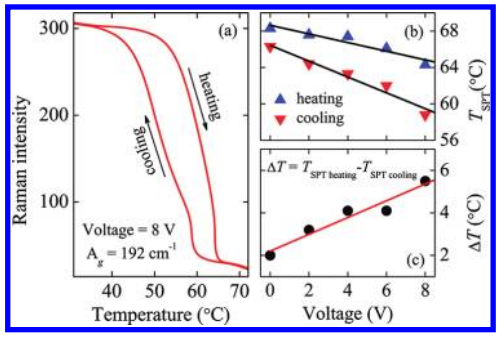

Figure 5. (a) Temperature vs relative Raman intensity of the A_g phonon mode at 192 cm^{-1} after background signal subtraction. Arrows on the curve denotes the temperature sweep directions. (b) Applied voltage dependence of the T_{SPT} is determined from Raman spectra. (c) The T_{SPT} delay corresponds to different applied voltages. The solid lines are the linearly fitting results to guide the eyes.

nanoparticles. Furthermore, the larger change of E_a at the high-temperature state can be ascribed to the fact that the volume-generated current dominates the free-carrier current injected from the electrode at the electric field.[11]

Raman Spectra and SPT for the Heating and Cooling Processes. Since the vibration modes of VO_2 nanoparticles are drastically different in the R and M phases, the Raman scattering technique allows us to independently monitor the electronic and structural transitions under an external electric field. The structures of VO_2 are based on an oxygen (O) bcc lattice with vanadium(V) in the octahedral sites, and the O octahedra are more or less regular. In the M phase, the unit cell doubles in size and the V^{4+} ions pair such that they twist to lower the symmetry. The M phase has a space group of $P2_1/c$ and 18 Raman-active phonons ($9A_g \oplus 9B_g$), exhibiting strong polarization dependence.[30] As an example, Figure 4a and b show the lattice vibrations of the VO_2 nanoparticles at the voltage of 8 V for the heating and cooling processes, respectively. The intense monoclinic A_g peaks can be observed at about 192, 222, 309, 388, and 615 cm^{-1}. The phonon frequencies appear in accordance with the previous Raman experimental reports.[30−33] Compared to the results observed by Kang et al. and Zhang et al.,[32,33] the absence of several phonon bands could be attributed to the different crystallinity and microstructure. Because of the large difference between V and O masses, the low-frequency A_g phonon modes at 192 and 222 cm^{-1} can be attributed to the motion of V-ions in the dimerized chains.[34] In addition, the weaker peaks located at near 260, 441, and 495 cm^{-1} could be assigned to the B_g phonon modes. It can be found that both the intensities of the A_g and B_g phonon modes decrease with increasing the temperature, and the B_g modes vanish with further increasing of the temperature. The variations of the relative intensities for the phonon peaks with the temperature before the SPT could be partly ascribed to the lattice temperature effects, which suggests a strong temperature dependence of the electronic behavior in the VO_2 nanoparticles.

When the temperature is heating up to 64.3 °C, all of the vibration modes related to the local structure of lower symmetry are softened and suddenly disappear due to a metallic R phase formed by the SPT. In particular, the complete disappearance of the 192 cm^{-1} peak at T_{SPT} indicates that the present VO_2 nanoparticles do not contain measurable amounts of the other oxide phase. For the cooling half-cycle, the temperature was ramped down from 100 °C to ensure the completion of that object's forward transition. Conversely, the vibration modes arise owing to the SPT when the temperature is cooling down to 58.8 °C. It indicates that the temperature for the onset of the reverse transition is clearly delayed by about 5.5 °C. Thus, one can conclude that the T_{SPT} of the VO_2 nanoparticles at the voltage of 8 V is 64.3 and 58.8 °C for the heating and cooling processes, respectively. Furthermore, there are no evident changes in the Raman peaks when the resistance undergoes a large jump, which confirms that the MIT occurs prior to the SPT. As we know, the changes of electronic and atomic structures play an important role in the SPT. At the low temperature, the d-orbit electrons are localized within the short V−V pairs. When the SPT occurs, the VO_2 structure shows an increased symmetry both in the V atomic chains and in the [VO_6] octahedron. The V−V pairs in the chains undergo the elongation of V−V1a and the shortening of V−V1b. As a result, the V ions are linearly aligned and the d electrons of V ions would be shared by all of the atoms in the chain. The delocalization of the d electrons among all V atoms and the change of the V−V distance induce the SPT.[16,35]

In order to characterize the variation of the phonon modes, the relative intensity of the Raman line at 192 cm^{-1} after background signal subtraction is displayed in Figure 5a. The phonon mode is chosen because it is relatively more identifiable in the quantitative way during the heating−cooling cycle. It can be found that the intensity of the vibration mode strongly depends on the temperature and shows a hysteresis behavior. The hysteresis loop of the relative intensity for the A_g phonon modes at 192 cm^{-1} is smaller than the hysteresis of the resistance measured simultaneously. In addition, the Raman phonon frequencies do not show an obvious variation trend with the temperature within the spectral resolution.

Electric Voltage Dependence of T_{SPT} and Its Applications. On the basis of the observation from Raman spectra, one can obtain the T_{SPT} of the VO_2 nanoparticles. The applied voltage dependence of the T_{SPT} is plotted in Figure 5b. At the heating process, the T_{SPT} decreases from 68.3 to 64.3 °C with the voltage increasing from 0 to 8 V. However, the T_{SPT} decreases from 66.3 to 58.8 °C for the cooling process with the same voltage. Moreover, the linearly fitting results reveal that the T_{SPT} decreases by −0.48 and −0.87 °C/V when heating and cooling across the SPT. It indicates that the T_{SPT} can be reasonably controlled by the applied electric voltage. A typical field effect transistor is composed of a gate layer, a dielectric layer, a semiconductor layer, and drain-source electrodes. The present three-terminal device

provides the basis for the proposed field effect transistor with the structure of bottom-gate/top-contact, as seen in Figure 1a. When the SPT occurs in the heating process, the band gap could rapidly be shorted from about 670 to 0 meV, resulting in weak optical absorption and high infrared reflectivity.[36] Thus, the device can be used as a programmable voltage switch by controlling the device under strong absorption (defined as 1) or high reflectivity (defined as 0) states with different applied voltages, which is tunable if required. Moreover, the device shows an excellent control over the electric resistance and the phase transition by the applied voltage with high sensitivity, quick response time, and good reproducibility, making it ideal for measuring the voltage in nanometer-scaled devices. It should be noted that the device was fabricated based on VO_2 nanoparticles rather than film formation. This is because nanoparticle structure can provide large areas of grain boundary and therefore wide current paths. The nanoscale interfacial boundary and strain further affect the hysteretic behavior of the transition. In addition, electric field lines converge around the nanoparticle site, and the intensity of the electric field at the tip of nanoparticle can greatly exceed that of the planar region. Hence, the carrier mobilities can be accelerated by strengthening the electrical field, and most of the carriers eventually reach the location of the nanoparticle due to the nanoscale-enhanced electrical field.[37] Nevertheless, the uniformity of the resistance values and stability of the SPT processes are improved using VO_2 nanoparticles, which is beneficial for the carrier density change and the SPT control by an external electric field.

As we know, an exponential decrease in the resistance with the temperature indicates a remarkable increase for free-carriers.[25,38] In the insulating M phase, the carriers are holes, and the V 3d band is strongly broadened as the temperature is increased. Two kinds of electron and hole carriers coexist in the intermediate phase, which still partially belongs to the M phase. However, the carriers are electrons in the tetragonal R structure, and the full metallic phase is formed. A change of carriers from the mixing of electrons and holes to electrons corresponds to the SPT. From the resistance measured, the resistance reduces with increasing the applied voltage, which indicates that the carrier densities increase with the voltage. Note that the carrier densities at critical point are given by $n_c(T,laser,V) = n(T) + n(laser) + n(V)$, where $n_c(T,laser,V)$ is the carrier densities excited by the temperature, laser, and electric field; $n(T)$, $n(laser)$, and $n(V)$ are the carrier densities excited by the temperature, laser, and electric field, respectively.[15] Therefore, the larger electric field will drive the electron densities exceeding a critical value and finally drive the change of carriers from the mixing of electrons and holes to electrons. Then, the intermediate phase is no longer thermodynamically stable. The VO_2 nanoparticles will undergo the SPT and transfer to the R phase, which contains the contributions from both the electron−phonon interaction between the lattice and the carriers as well as the Coulomb interaction between carriers at a given lattice site.[27]

However, the knowledge of semiconductor physics could be useful to interpret the phenomenon of the electric field assisted SPT. When a small positive voltage is applied, the positive charges appear in the surface of VO_2 nanoparticles. The generated electric field through the device will pull the electrons (minority carriers) to the VO_2 layer and push the holes (majority carriers) away from the VO_2 layer. Undoubtedly, the number of electrons accumulated at the surface of VO_2 is remarkably larger than that of the holes when a larger positive voltage is applied. Therefore, the increase of electron densities with increasing positive voltage promotes the transition from the M to R structure, resulting in the decrease of the T_{SPT} with the applied voltage.

One can also understand the electric field effects on the SPT from the perspective of the electronic band structure. In M phase VO_2 nanoparticles, the crystal field splits the degenerate d orbitals into t_{2g} bands and e_g^{σ} bands. The t_{2g} bands are further split into a lower a_{1g} band and upper e_g^{π} bands. The $V^{4+}-V^{4+}$ pairing along the c axis splits the a_{1g} band into lower and upper a_{1g} bands. Moreover, the twisting of the $V^{4+}-V^{4+}$ pairs increases V_d-O_p hybridization and lifts the e_g^{π} band above the Fermi energy (E_F) so that only the lower a_{1g} band is filled. The band gap energy of the M phase corresponds to an indirect transition from the top of the filled a_{1g} band (E_v) to the bottom of the empty e_g^{π} band (E_c). In the R phase, the tetragonal crystal field splits the t_{2g} bands into an a_{1g} band, formed by σ bonding between two adjacent V^{4+} ions along the c axis, and e_g^{π} bands formed by the V_d-O_p antibonding doublet. The a_{1g} band overlaps the e_g^{π} band with a zero band gap.[39−41] When a positive voltage is applied, the E_c band will bend toward the E_F band and the intrinsic level E_i is close to the E_F. Hence, the increasing of the electric voltage could offer a driving force for moving the E_c band across the E_v band and changing the lattice constant by shortening the V−V distance. Nevertheless, the density of states increases exponentially with increasing the electric field, and the E_a decreases with increasing the voltage, which could be another possible cause for the applied voltage dependence of the SPT.

Influences of Applied Voltage on the T_{SPT} Delay. The T_{SPT} delay (ΔT_{SPT}) between the heating and cooling processes without an external electric field has been reported by many groups.[42,43] As shown in Figure 5b, the same delayed phenomenon can be also observed from the present results. However, our further study reveals that the ΔT_{SPT} is strongly affected by the applied voltage and increases with increasing the electric voltage, as presented in Figure 5c. Furthermore, the linearly fitting result suggests that the ΔT_{SPT} increases by 0.4 °C/V with increasing the applied voltage. When the temperature is decreased back down, the hole carriers do not immediately generate, resulting in the transition delay. As discussed previously, the external electric field can pull the electrons and push the holes. Thus, the increasing of the applied voltage will make the generation of holes more difficult, which finally results in the observed voltage dependence of ΔT_{SPT}. Finally, it is clearly shown in Figure 1b that the VO_2 nanoparticles contains multiple grains in the gating device and a percolative behavior would be expected during the phase transition. This behavior can explain why both the electronic transition (Figure 2) and the structural transition (Figure 5) are broadened. Although the T_{SPT} can be reduced for wider applications by increasing the electric voltage, the power consumption will increase at the same time and the reset of the device and/or switch could be more difficult due to the T_{SPT} delay with the voltage. For the practical applications, one should sufficiently consider the relationship among the above impact factors.

CONCLUSIONS

In summary, the VO_2 nanoparticles have been fabricated on the $SiO_2/Si(100)$ substrate using direct-current magnetron sputtering. Electric measurements of the VO_2 three-terminal device reveal that the MIT occurs prior to the SPT, and the

transition temperatures are strongly affected by the external electric field. The estimated values of the activation energy at the low-temperature state are remarkably larger than that at the high-temperature state and decrease with increasing the voltage. The temperature dependence of the vibration modes with the voltage varied from 0 to 8 V has been measured and uniquely assigned. The relative intensity of the A_g phonon modes at 192 cm^{-1} shows a hysteresis behavior. Moreover, the T_{SPT} decreases about 4 and 7.5 °C for the heating and cooling processes, respectively, with increasing the voltage from 0 to 8 V. The T_{SPT} delay is increased by 0.4 °C/V with increasing the applied voltage. The present study shows an instructive method to reduce the T_{SPT} and could lead to a deeper understanding of the structural phase transition in VO_2 nanoparticles.

AUTHOR INFORMATION

Corresponding Author
*E-mail: zghu@ee.ecnu.edu.cn.

ACKNOWLEDGMENT

We acknowledge Professor Zheng Tang, Xiao Chen, Xiangui Chen, and Zhenni Zhan for their helpful discussions and technical support. This work was financially supported by the Natural Science Foundation of China (grant nos. 60906046 and 11074076), Major State Basic Research Development Program of China (grant nos. 2007CB924901, 2007CB924904, and 2011CB922200), Program of New Century Excellent Talents, MOE (grant no. NCET-08-0192) and PCSIRT, Projects of Science and Technology Commission of Shanghai Municipality (grant nos. 10DJ1400201, 10SG28, 10ZR1409800, and 09ZZ42), and the Program for Professor of Special Appointment (Eastern Scholar) at Shanghai Institutions of Higher Learning. W.W.L. thanks ECNU Fostering Project for National Top Hundred Doctoral Dissertations (grant no. PY2011014).

REFERENCES

(1) Qazilbash, M. M.; Brehm, M.; Chae, B. G.; Ho, P. C.; Andreev, G. O.; Kim, B. J.; Yun, S. J.; Balatsky, A. V.; Maple, M. B.; Keilmann, F.; Kim, H. T.; Basov, D. N. *Science* **2007**, *318*, 1750.
(2) Booth, J. M.; Casey, P. S. *ACS. Appl. Mater. Interfaces* **2009**, *1*, 1899.
(3) Mannhart, J.; Schlom, D. G. *Science* **2010**, *327*, 1607.
(4) Corr, S. A.; Shoemaker, D. P.; Melot, B. C.; Seshadri, R. *Phys. Rev. Lett.* **2010**, *105*, 056404.
(5) Lu, S. W.; Hou, L. S.; Gan, F. X. *Adv. Mater.* **1997**, *9*, 244.
(6) Whittaker, L.; Jaye, C.; Fu, Z. G.; Fischer, D. A.; Banerjee, S. *J. Am. Chem. Soc.* **2009**, *131*, 8884.
(7) Cao, J.; Fan, W.; Chen, K.; Tamura, N.; Kunz, M.; Eyert, V.; Wu, J. *Phys. Rev. B* **2010**, *82*, 241101R.
(8) Mlyuka, N. R.; Niklasson, G. A.; Granqvist, C. G. *Appl. Phys. Lett.* **2009**, *95*, 171909.
(9) Sohn, J. I.; Joo, H. J.; Ahn, D.; Lee, H. H.; Porter, A. E.; Kim, K.; Kang, D. J.; Welland, M. E. *Nano Lett.* **2009**, *9*, 3392.
(10) Cao, J.; Ertekin, E.; Srinivasan, V.; Fan, W.; Huang, S.; Zheng, H.; Yim, J. W. L.; Khanal, D. R.; Ogletree, D. F.; Grossman, J. C.; Wu, J. *Nat. Nanotechnol.* **2009**, *4*, 732.
(11) Ko, C.; Ramanathan, S. *Appl. Phys. Lett.* **2008**, *93*, 252101.
(12) Kim, H. T.; Chae, B. G.; Youn, D. H.; Kim, G.; Kang, K. Y.; Lee, S. J.; Kim, K.; Lim, Y. S. *Appl. Phys. Lett.* **2005**, *86*, 242101.
(13) Yang, Z.; Ko, C.; Ramanathan, S. *J. Appl. Phys.* **2010**, *108*, 073708.
(14) Xie, R. G.; Bui, C. T.; Varghese, B.; Zhang, Q. X.; Sow, C. H.; Li, B. W.; Thong, J. T. L. *Adv. Funct. Mater.* **2011**, *21*, 1602.
(15) Kim, H. T.; Lee, Y. W.; Kim, B. J.; Chae, B. G.; Yun, S. J.; Kang, K. Y.; Han, K. J.; Yee, K. J.; Lim, Y. S. *Phys. Rev. Lett.* **2006**, *97*, 266401.
(16) Yao, T.; Zhang, X. D.; Sun, Z. H.; Liu, S. J.; Huang, Y. Y.; Xie, Y.; Wu, C. Z.; Yuan, X.; Zhang, W. Q.; Wu, Z. Y.; Pan, G. Q.; Hu, F. C.; Wu, L. H.; Liu, Q. H.; Wei, S. Q. *Phys. Rev. Lett.* **2010**, *105*, 226405.
(17) Kim, B. J.; Lee, Y. W.; Chae, B. G.; Yun, S. J.; Oh, S. Y.; Kim, H. T.; Lim, Y. S. *Appl. Phys. Lett.* **2007**, *90*, 023515.
(18) Wu, J. Q.; Gu, Q.; Guiton, B. S.; de Leon, N. P.; Ouyang, L.; Park, H. *Nano Lett.* **2006**, *6*, 2313.
(19) Wei, J.; Wang, Z.; Chen, W.; Cobden, D. H. *Nat. Nanotechnol.* **2009**, *4*, 420.
(20) Appavoo, K.; Haglund, R. F., Jr. *Nano Lett.* **2011**, *11*, 1025.
(21) Hu, B.; Ding, Y.; Chen, W.; Kulkarni, D.; Shen, Y.; Tsukruk, V. V.; Wang, Z. L. *Adv. Mater.* **2010**, *22*, 5134.
(22) Donev, E. U.; Lopez, R.; Feldman, L. C.; Haglund, R. F., Jr. *Nano Lett.* **2009**, *9*, 702.
(23) Li, W. W.; Zhu, J. J.; Xu, X. F.; Jiang, K.; Hu, Z. G.; Zhu, M.; Chu, J. H. *J. Appl. Phys.* **2011**, *110*, 013504.
(24) Liang, J. R.; Hu, M.; Wang, X. D.; Li, G. K.; Ji, A.; Yang, F. H.; Liu, J.; Wu, N. J.; Chen, H. D. *Acta Phys.-Chim. Sin.* **2009**, *25*, 1523.
(25) Kim, H. T.; Chae, B. G.; Youn, D. H.; Maeng, S. L.; Kim, G.; Kang, K. Y.; Lim, Y. S. *New J. Phys.* **2004**, *6*, 52.
(26) Tselev, A.; Meunier, V.; Strelcov, E.; Shelton, W. A., Jr.; Luk'yanchuk, I. A.; Jones, K.; Proksch, R.; Kolmakov, A.; Kalinin, S. V. *ACS Nano* **2010**, *4*, 4412.
(27) Zhang, S. X.; Chou, J. Y.; Lauhon, L. J. *Nano Lett.* **2009**, *9*, 4527.
(28) Mun, B. S.; Chen, K.; Leem, Y.; Dejoie, C.; Tamura, N.; Kunz, M.; Liu, Z.; Grass, M. E.; Park, C.; Yoon, J.; Lee, Y. Y.; Ju, H. *Phys. Status Solidi RRL* **2011**, *5*, 107.
(29) Shin, Y.; Moon, J.; Ju, H. *J. Korean Phys. Soc.* **2008**, *52*, 1828.
(30) Chen, C. H.; Wang, R. F.; Shang, L.; Guo, C. F. *Appl. Phys. Lett.* **2008**, *93*, 171101.
(31) Schilbe, P. *Phys. B* **2002**, *316-317*, 600.
(32) Kang, L. T.; Gao, Y. F.; Zhang, Z. T.; Du, J.; Cao, C. X.; Chen, Z.; Luo, H. J. *J. Phys. Chem. C* **2010**, *114*, 1901.
(33) Zhang, Z. T.; Gao, Y. F.; Chen, Z.; Du, J.; Cao, C. X.; Kang, L. T.; Luo, H. J. *Langmuir* **2010**, *26*, 10738.
(34) Arcangeletti, E.; Baldassarre, L.; Di Castro, D.; Lupi, S.; Malavasi, L.; Marini, C.; Perucchi, A.; Postorino, P. *Phys. Rev. Lett.* **2007**, *98*, 196406.
(35) Wu, C. Z.; Wei, H.; Ning, B.; Xie, Y. *Adv. Mater.* **2010**, *22*, 1972.
(36) Liu, W. T.; Cao, J.; Fan, W.; Hao, Z.; Martin, M. C.; Shen, Y. R.; Wu, J.; Wang, F. *Nano Lett.* **2011**, *11*, 466.
(37) Liu, Q.; Long, S. B.; Wang, W.; Tanachutiwat, S.; Li, Y. T.; Wang, Q.; Zhang, M. H.; Huo, Z. L.; Chen, J. N.; Liu, M. *IEEE Electron Device Lett.* **2010**, *31*, 1299.
(38) Ruzmetov, D.; Heiman, D.; Claflin, B. B.; Narayanamurti, V.; Ramanathan, S. *Phys. Rev. B* **2009**, *79*, 153107.
(39) Chen, C. H.; Fan, Z. Y. *Appl. Phys. Lett.* **2009**, *95*, 262106.
(40) Qazilbash, M. M.; Schafgans, A. A.; Burch, K. S.; Yun, S. J.; Chae, B. G.; Kim, B. J.; Kim, H. T.; Basov, D. N. *Phys. Rev. B* **2008**, *77*, 115121.
(41) Eyert, V. *Ann. Phys.* **2002**, *11*, 650.
(42) Frenzel, A.; Qazilbash, M. M.; Brehm, M.; Chae, B. G.; Kim, B. J.; Kim, H. T.; Balatsky, A. V.; Keilmann, F.; Basov, D. N. *Phys. Rev. B* **2009**, *80*, 115115.
(43) Kim, J.; Ko, C.; Frenzel, A.; Ramanathan, S.; Hoffman, J. E. *Appl. Phys. Lett.* **2010**, *96*, 213106.